Pakistan Veterinary Journal

ISSN: 0253-8318 (PRINT), 2074-7764 (ONLINE)
DOI: 10.29261/pakvetj/2026.197

RESEARCH ARTICLE

Jiawei Gegen Qinlian Decoction Ameliorates DSS-Induced Ulcerative Colitis by Restoring Intestinal Barrier Integrity Via the Gut Microbiota–Metabolite Axis

Qinhong Yang[1,3#], Wanying Zhang[1#], Xianbo Cheng[2#], Xingjian Yu[5], Junjun He[3,6], Xiaonan Yang[4*] and Qiu Zhong[1*]

[1]Guangxi Key Laboratory of Animal Breeding, Disease Control and Prevention, College of Animal Science and Veterinary Medicine, Guangxi University, Nanning, Guangxi 530000, China; [2]Dietary Fiber Isolation and Structural Characterization Laboratory, Guangxi Technology and Business Vocational College, Nanning 530000, China; [3]College of Traditional Chinese Medicine, Yunnan University of Chinese Medicine, Kunming 650500, China; [4]National Engineering Research Centre for Southwest Endangered Medicinal Resources Development, Guangxi Botanical Garden of Medicinal Plants, Nanning, Guangxi 530023, China; [5]Department of biochemistry and molecular medicine, University of California, Davis, Sacramento, CA, 95817, USA; [6]The Yunnan Key Laboratory of Veterinary Etiological Biology, College of Veterinary Medicine, Yunnan Agricultural University, Kunming 650201, Yunnan Province, China.
[#]These authors contributed equally to this article
*Corresponding author: zhongqiujob@163.com (QZ); nannangood33@163.com (XY)

ARTICLE HISTORY (26-565)

Received: May 11, 2026
Revised: July 15, 2026
Accepted: August 5, 2026
Published online: August 16, 2026

Key words:
Gut microbiota
Intestinal barrier integrity
Jiawei Gegen Qinlian Decoction (JGQD)
Metabolomics
Ulcerative colitis (UC)

ABSTRACT

Ulcerative colitis (UC) is a multifactorial intestinal inflammatory disorder involving excessive immune activation, oxidative imbalance, epithelial barrier impairment, microbial disturbance, and metabolic dysregulation. Similar pathological alterations are commonly encountered in animal intestinal diseases, emphasizing the exploration of safe and effective natural therapeutics. This study aimed to clarify the protective actions and potential mechanisms of Jiawei Gegen Qinlian Decoction (JGQD) against dextran sulfate sodium (DSS)-induced colitis. A comprehensive strategy combining network pharmacology, *in-vivo* validation, 16S rRNA gene sequencing and UHPLC-MS metabolomics was applied to characterize the regulatory effects of JGQD on therapeutic targets, inflammatory status, oxidative damage, intestinal barrier function, microbial composition, and fecal metabolic alterations. Network analysis revealed that JGQD-associated targets were mainly involved in inflammation-regulating pathways, including TNF, NF-κB, PI3K-Akt, MAPK and JAK-STAT signaling cascades. In DSS-challenged mice, JGQD markedly decreased markedly by colonic TNF-α, IL-6, IL-1β, MDA and MPO levels, while enhancing IL-10 production, SOD activity and total antioxidant capacity. Moreover, JGQD restored tight junction protein expression (ZO-1, Occludin and Claudin-3), reshaped gut microbial composition with increased Akkermansia abundance and modulated metabolism associated with amino acids, bile acids and lipids. JGQD alleviated experimental colitis by regulating the interconnected microbiota–metabolite–intestinal barrier network, suggesting its potential application as a natural multi-component intervention for controlling intestinal inflammatory disorders and maintaining barrier homeostasis in veterinary medicine.

To Cite This Article: Yang Q, Zhang W, Cheng X, Guo Y, Yu X, He J, Yang X and Zhong Q, 2026. Jiawei gegen qinlian decoction ameliorates dss-induced ulcerative colitis by restoring intestinal barrier integrity via the gut microbiota–metabolite axis. Pak Vet J, 46(8): 2095-2107. http://dx.doi.org/10.29261/pakvetj/2026.197

INTRODUCTION

Ulcerative colitis (UC) is a persistent inflammatory bowel condition marked by ongoing mucosal inflammation and gradual deterioration of colonic functionality. The lesions often start in the rectum and extend proximally throughout the colon in a continuous distribution. Abdominal pain, diarrhoea, weight loss, fatigue, mucus and bloody stools, and abdominal pain are among the most prevalent clinical manifestations (Ungaro *et al*., 2017; Perler *et al*., 2019). UC is generally regarded as a multifactorial disorder, which includes immune dysregulation, sustained inflammatory activation, epithelial barrier dysfunction, genetic

susceptibility, environmental factors, and gut microbiota disturbance, even though its precise etiology remains unclear (Ungaro *et al*., 2017; Shahgoli *et al*., 2024). Persistent intestinal inflammation represents a considerable clinical concern in animals from a veterinary standpoint. In companion animals, particularly dogs, chronic enteropathy is characterized by persistent gastrointestinal symptoms, mucosal immune dysregulation, intestinal inflammation and altered microbiome–host interactions. This condition is like human inflammatory bowel disease in terms of mucosal immune activation, epithelial barrier dysfunction, and gut microbiota dysbiosis (Jergens and Heilmann, 2022; Kaga *et al*., 2024). Therefore, although experimental UC models cannot fully reproduce naturally occurring chronic enteropathies in animals, they provide valuable mechanistic references for understanding intestinal inflammation and developing potential intervention strategies in veterinary medicine. Promoting mucosal repair and restoring barrier integrity have become crucial therapeutic strategies for UC management because intestinal mucosal barrier disruption is one of the pathological features of UC that is thought to be a crucial event in the disease's initiation and progression (Zong *et al*., 2023; Wu *et al*., 2025).

Intestinal disorders in cattle and experimental animals are often linked to impaired epithelial barrier function. The intestinal barrier constitutes a multifaceted defense mechanism comprising physical, chemical, immunological and microbiological elements, with the epithelial barrier serving as the principal protective contact against luminal threats. The intestinal epithelial cells' intercellular junctional complexes are principally responsible for its maintenance. Tight junctions (TJs) are critical components of the intestinal epithelial barrier that maintains mucosal integrity, thereby regulating paracellular permeability. Transmembrane proteins, including occludin and claudins, as well as zonula occludins (ZO) scaffold proteins (ZO-1, ZO-2 and ZO-3), provide structural integrity for epithelial barrier function in tight junctions (Prasad *et al*., 2005; Ungaro *et al*., 2017; Shahgoli *et al*., 2024). Through interactions with the cytoskeletal network, TJ proteins regulate paracellular permeability and maintain epithelial barrier stability. In the realm of UC, the expression and distribution of TJ protein are compromised due to aberrant signaling pathways and heightened inflammatory responses, resulting in augmented intestinal permeability, increased translocation of bacteria and endotoxins, and further exacerbation of mucosal inflammation and damage (Zong *et al*., 2023; Wu *et al*., 2025).

Maintaining intestinal homeostasis, controlling immunity and preserving barrier function all depend on the gut microbiota (Zong *et al*., 2023; Wu *et al*., 2025; Huang *et al*., 2026). Dysbiosis of gut microbiota is a characteristic feature of ulcerative colitis, typically linked to a diminished presence of advantageous commensals, proliferation of opportunistic pathogens and a reduction in microbial diversity. This microbial dysbiosis is associated with diminished synthesis of advantageous metabolites, especially short-chain fatty acids (SCFAs), which are crucial for preserving intestinal barrier integrity and modulating host immunological equilibrium (Parada *et al*., 2019; Abraham *et al*., 2022; Loh *et al*., 2024). Microbial dysbiosis contributes to UC progression through activation of pattern recognition receptors, induction of inflammatory cytokine production, oxidative stress responses, and disruption of mucosal integrity (Abraham *et al*., 2022). In addition, microbiota-derived or microbiota-modulated metabolites—including SCFAs, bile acid derivatives, amino acid metabolites, and arachidonic acid-related lipids—act as important mediators of host–microbiota interactions, directly influencing immune responses and tight junction stability. Alterations in these metabolic profiles are closely associated with disease activity and progression (Yao *et al*., 2021; Sharma *et al*., 2025).

Traditional Chinese medicine (TCM) preparations have been extensively utilized for the prophylaxis and management of intestinal inflammatory disorders due to their diverse bioactive components that can concurrently modulate many pathogenic mechanisms (Wang *et al*., 2024; Xu *et al*., 2025). The accumulation of evidence suggests that TCM formulations have protective effects against intestinal inflammation through a variety of mechanisms, such as the regulation of gut microbial composition and metabolism, the restoration of epithelial barrier function and the promotion of mucosal repair (Liu *et al*., 2022; Meng *et al*., 2024; Bi *et al*., 2025; Wang *et al*., 2026). The traditional prescription Gegen Qinlian Decoction, which was first documented in the classical medical text Shanghan Lun, is widely used to treat damp-heat diarrhea. It has been extensively investigated in experimental and clinical investigations of treating UC, and previous studies have shown that it possesses heat-clearing, anti-inflammatory, and antidiarrheal effects (Zhao *et al*., 2021; Hu *et al*., 2024). Thus, examining the protective properties of Gegen Qinlian Decoction against intestinal inflammation could provide significant insights for creating natural, multi-faceted, and non-antibiotic approaches to intestinal health management in veterinary practice.

Based on the classical compatibility principles of Xianglian Pill (“clearing heat, regulating qi, and relieving pain”) (Yang *et al*., 2024) and Baitouweng Decoction (“clearing heat and toxins, relieving dysentery and protecting the intestine”) (Pan *et al*., 2024), Aucklandiae Radix and Fraxini Cortex were incorporated into the original Gegen Qinlian Decoction and combined with Glycyrrhizae Radix et Rhizoma to formulate Jiawei Gegen Qinlian Decoction (JGQD). This modified prescription is expected to retain the anti-inflammatory and antidiarrheal properties of the original formula while more comprehensively addressing the complex pathological features of modern UC. This research sought to elucidate the pathways that contribute to the protective properties of JGQD against UC by a comprehensive approach involving network pharmacology, animal studies, microbiome analysis and metabolomics. Network pharmacology was utilized to forecast possible active substances, targets and signaling pathways, subsequently validated in a DSS-induced colitis murine model. The regulatory impacts of JGQD on inflammation, oxidative stress, intestinal barrier integrity and the gut microbiota–metabolite relationship were further examined using 16S rRNA sequencing and metabolomic analysis.

MATERIALS AND METHODS

Drugs and reagents: DSS (40 kDa), mesalazine (5-ASA), ELISA kits for IL-6, IL-10, IL-1β and TNF-α, and commercial kits for SOD, MDA, CAT and MPO were acquired from Ambeed, Yeasen Biotechnology, Nanjing Boyan Biotechnology and Solarbio Biotechnology, respectively. ZO-1, Occludin, Claudin-3, β-actin, and α-tubulin antibodies were procured from Proteintech. Servicebio, Boster Biological Technology and ABclonal Biotechnology provided the H&E staining reagents, RIPA lysis buffer and BCA protein assay kits, respectively. Radix Puerariae, Scutellariae Radix, Fraxini Cortex, Aucklandiae Radix and Glycyrrhizae Radix et Rhizoma were the crude botanicals used to create JGQD, which was purchased from the Yunnan Traditional Chinese Medicine Market in Yunnan, China.

Animals: Male BALB/c rodents (6–8 weeks old) were procured from Beijing SPF Biotechnology Co., Ltd. (Beijing, China; License No. SCXK (Jing) 2024-0001). The procedures were conducted in accordance with the institutional guidelines for laboratory animal care, and the Animal Ethics Committee of the College of Animal Science and Veterinary Medicine, Guangxi University reviewed and approved all procedures involving animals (Approval No. GXU-2026-172).

Preparation of JGQD: The conventional water decoction method was employed to prepare JGQD. In brief, the herbal mixture (Radix Puerariae 15gm, Scutellariae Radix 9gm, Fraxini Cortex 9gm, Aucklandiae Radix 10gm, Glycyrrhizae Radix et Rhizoma 6gm) was washed with distilled water and immersed in 5 volumes of distilled water (w/v) for 1 hour at ambient temperature. The aqueous extract was obtained by filtration after the mixture was decocted for 1 hour. The residual herbal material was re-extracted under identical conditions for an additional 30 minutes. The final crude drug concentration of 1g/mL was achieved by concentrating the amalgamated filtrates under diminished pressure. The concentration was then portioned and stored at −80°C until it was needed.

Network pharmacology analysis: Compounds associated with JGQD were sourced from the TCMSP database, and potential candidates were selected based on oral bioavailability (OB>30%) and drug-likeness (DL≥0.18) for further examination. The UniProt database was employed to standardize compound-target relationships, while the GeneCards, OMIM, TTD and DisGeNET repositories were consulted to identify ulcerative colitis-related targets. In Cytoscape (version 3.7.1), intersection targets were identified as potential therapeutic targets and are employed to establish herb–compound–target network. The overlapping targets were uploaded into the STRING database to create a PPI network, with Homo sapiens as the reference organism with a minimum interaction confidence threshold of 0.4. The BisoGenet and CytoNCA modules were employed to conduct network topology analysis to identify hub genes. The DAVID database was employed for Gene Ontology annotation and KEGG pathway enrichment analysis, with the resultant biological functions and signaling pathways shown using the Micro-bioinformatics web platform.

Experimental design: After a week of adaptation, 72 mice were randomly allocated into six groups (12 mice each): CON, MOD, PC, JGQD-L, JGQD-M and JGQD-H. Experimental colitis was elicited in all groups except from the control group by administering drinking water containing 3% (w/v) DSS for a duration of 7 days. Mice in the JGQD cohorts were administered JGQD orally at dosages of 3.64, 7.28, or 14.56gm/kg/day, whilst the CON and MOD groups were given saline by gavage (200μL/day). Mesalazine was given to the PC group at a dosage of 100mg/kg every day. Interventions were administered on daily basis throughout the treatment phase (Fig. 2A).

Assessment of physiological parameters: The disease activity index (DAI) was determined by monitoring clinical indications, such as body weight, stool consistency and rectal hemorrhage, daily. Blood, fecal samples, and colon tissues were collected after the rodents were euthanized after the 7-day intervention. Recording colon length served as an indicator of disease severity. The colon specimens that were intended for histological examination were cleansed with PBS and fixed in 4% paraformaldehyde. The remaining tissues and faecal samples were subjected to biochemical, microbiota, and metabolomic analyses after being stored at −80°C.

Histopathological analysis (H&E Staining): Colon specimens were preserved in 4% paraformaldehyde for 48 hours, thereafter, treated for paraffin embedding, and sliced to a thickness of 5μM. Histological alterations were evaluated by H&E staining, then analyzed via light microscopy.

Determination of inflammatory cytokines and oxidative stress markers: The manufacturers' instructions were followed to produce serum and colon tissue homogenates. Supernatants were extracted for biochemical detection following centrifugation. Commercial ELISA assays were employed to quantify the concentrations of IL-6, IL-1β, IL-10 and TNF-α. The concentrations of oxidative stress indicators, such as SOD, MDA, MPO and T-AOC, were assessed utilizing commercially available assay kits in accordance with the manufacturers' instructions.

Immunofluorescence staining: Colon sections fixed in paraffin underwent immunofluorescence analysis for ZO-1, Occludin, and Claudin-3. Following antigen retrieval using a citrate buffer (pH 6.0), the sections were permeabilized and subjected to BSA blocking prior to overnight incubation with primary antibodies at 4°C. Nuclei were counterstained with DAPI following incubation with fluorescently labelled secondary antibodies. Fluorescence intensity was quantified using image analysis software after images were acquired using a fluorescence microscope with identical exposure settings.

Western blot analysis: Colon tissues were disrupted in RIPA buffer, and protein levels were quantified utilizing a bicinchoninic acid (BCA) test kit. Identical quantities of protein (20μg) were separated using 12% SDS-PAGE and

subsequently transferred to PVDF membranes. After blocking, the membranes were subjected to an overnight incubation at 4°C with primary antibodies targeting ZO-1, Occludin and Claudin-3, succeeded by HRP-conjugated secondary antibodies. Immunoreactive bands were identified by an advanced chemiluminescence technique and measured via densitometry utilizing ImageJ software. GAPDH functioned as the loading control.

16S rRNA gene amplicon sequencing analysis: Faecal microbial DNA was isolated utilizing the E.Z.N.A.® Stool DNA Kit (Omega Bio-Tek, USA). The V3–V4 segment of the bacterial 16S rRNA gene was amplified using the 338F/806R primer combination and sequenced utilizing an Illumina NextSeq 2000 platform. Sequence data were analyzed using the Majorbio Cloud Platform utilizing the QIIME2 framework, with DADA2 used for quality assessment, noise reduction and amplicon sequence variant (ASV) creation. The taxonomic categorization of ASVs was conducted using the SILVA reference database. Microbial diversity was measured by alpha- and beta-diversity assessments, whereas variations in community composition among groups were analyzed using permutational multivariate analysis of variance (PERMANOVA). Differentially abundant taxa were discerned by linear discriminant analysis effect size (LEfSe), with a significant threshold set at an LDA score of 2 and P values below 0.05.

Metabolomics analysis: Fecal metabolites were centrifuged at 13,000×g for 15 minutes at 4°C after being extracted under low-temperature conditions. The supernatants were subjected to analysis using a UHPLC–Orbitrap Exploris 240 mass spectrometry system (Thermo Scientific, USA). The Majorbio Cloud Platform was employed to process metabolomic data. Progenesis QI (version 3.0, Waters, USA) was employed to perform peak extraction, alignment, normalization, and metabolite annotation. The MS/MS spectrum data was contrasted with records in the HMDB and METLIN databases for the purpose of metabolite identification. PCA and OPLS-DA were utilized to assess the differentiation of overall metabolic profiles among the experimental cohorts. Metabolites with substantial alterations were chosen based on VIP values exceeding 1 and P values below 0.05, thereafter undergoing KEGG pathway analysis to identify the relevant metabolic pathways.

Statistical analysis: Data are presented as mean ± standard error of the mean (SEM). Statistical evaluations were conducted utilizing GraphPad Prism 10.1.2 (GraphPad Software, USA). Variations between groups were assessed using ANOVA, succeeded by relevant post hoc analyses. A P value of less than 0.05 was deemed statistically significant, with *P<0.05, **P<0.01 and ***P<0.001 representing the corresponding levels of significance.

RESULTS

Network pharmacology analysis of JGQD: A total of 137 potential chemical constituents of JGQD were discovered from the TCMSP database, comprising 92 compounds from Glycyrrhizae Radix et Rhizoma, 4 from Radix Puerariae, 32 from Scutellariae Radix, 6 from Aucklandiae Radix and 3 from Fraxini Cortex. A total of 4,100 genes that are associated with UC were obtained from public disease databases, including GeneCards. These genes were intersected with the predicted targets of JGQD, resulting in 170 shared targets. This implies that they might have a role in the therapeutic benefits of JGQD for UC (Fig. 1A). A network of "herb–compound–target" interactions was created, including 305 nodes and 1,832 edges, derived from the identified active compounds and shared targets (Fig. 1B). The chemicals quercetin, β-sitosterol, kaempferol, formononetin, and wogonin exhibit the highest values, suggesting their significant significance in the therapeutic efficacy of JGQD against UC. PPI analysis of the 170 shared targets generated a network containing 170 nodes and 1,693 interactions (Fig. 1C). AKT1, IL6, TNF, TP53 and IL1β exhibited the highest Degree, Betweenness Centrality and Closeness Centrality values in the topological analysis conducted using Cytoscape (version 3.7.1). This suggests that these genes occupy central positions within the interaction network.

GO enrichment analysis indicated that the common targets were markedly linked to functional categories related to immune modulation, tissue repair, oxidative stress and inflammatory responses (Fig. 1D). Biological process analysis highlighted responses to lipopolysaccharide and bacterial-derived molecules, wound healing and oxidative stress. Cellular component analysis showed significant enrichment in membrane rafts, membrane microdomains, protein kinase complexes and transcription regulator complexes, whereas molecular function analysis mainly involved transcription factor binding, nuclear receptor activity, and cytokine receptor binding. Hub genes, including AKT1, IL6, TNF, and TP53, were represented in several enriched functional categories.

KEGG analysis identified 267 enriched pathways, including 39 pathways associated with UC (Fig. 1E). The top 15 enriched pathways were selected for visualization. The common objectives were mostly linked to inflammatory and immunological reactions, signal transduction mechanisms, and metabolic pathways. The TNF and PI3K-Akt signaling pathways showed the greatest enrichment, while NF-κB, MAPK, NOD-like receptor, Toll-like receptor, JAK-STAT, autophagy, mTOR, AMPK, PPAR signaling, arachidonic acid metabolism, bile secretion, and tryptophan metabolism were also significantly enriched

JGQD attenuates DSS-induced colonic injury in mice: Mice in the CON group remained healthy throughout the experiment, exhibiting glossy fur, normal food intake, continuous body weight gain and normal activity (Fig. 2B; Fig. 2C). In contrast to the CON group, mice subjected to DSS exhibited characteristic colitis-like symptoms, such as lethargy, ruffled fur, diarrhoea, and hematochezia, alongside considerable weight loss (P<0.001). In contrast, treatment with mesalazine (PC) or JGQD at different doses (JGQD-L, JGQD-M and JGQD-H) significantly alleviated these clinical manifestations and promoted body weight recovery compared with the MOD group

(P<0.001). DAI scores were consistently significantly lower in all treatment groups than in the MOD group (P<0.001). The colons of MOD mice were significantly shorter and darker in appearance than those of the CON group, as evidenced by a gross examination (Fig. 2D; Fig. 2E). Colon length was significantly reduced following DSS administration (P<0.001), whereas treatment with mesalazine, JGQD-M, or JGQD-H significantly attenuated DSS-induced colon shortening (P<0.001). These findings were additionally corroborated by histopathological analysis (Fig. 2F). In the CON group, the colonic crypt architecture was unaltered (yellow dashed line), and goblet cells were abundant and arrayed in a regular pattern (yellow arrows). In contrast, the MOD group exhibited depletion of goblet cells, prominent lymphocyte infiltration, and severe crypt destruction (green arrows). The pathological alterations were significantly ameliorated in the PC and JGQD-treated groups. The JGQD-L, JGQD-M and JGQD-H groups all exhibited a dose-dependent enhancement. The JGQD-H group exhibited the most pronounced protective effect at the highest dosage.

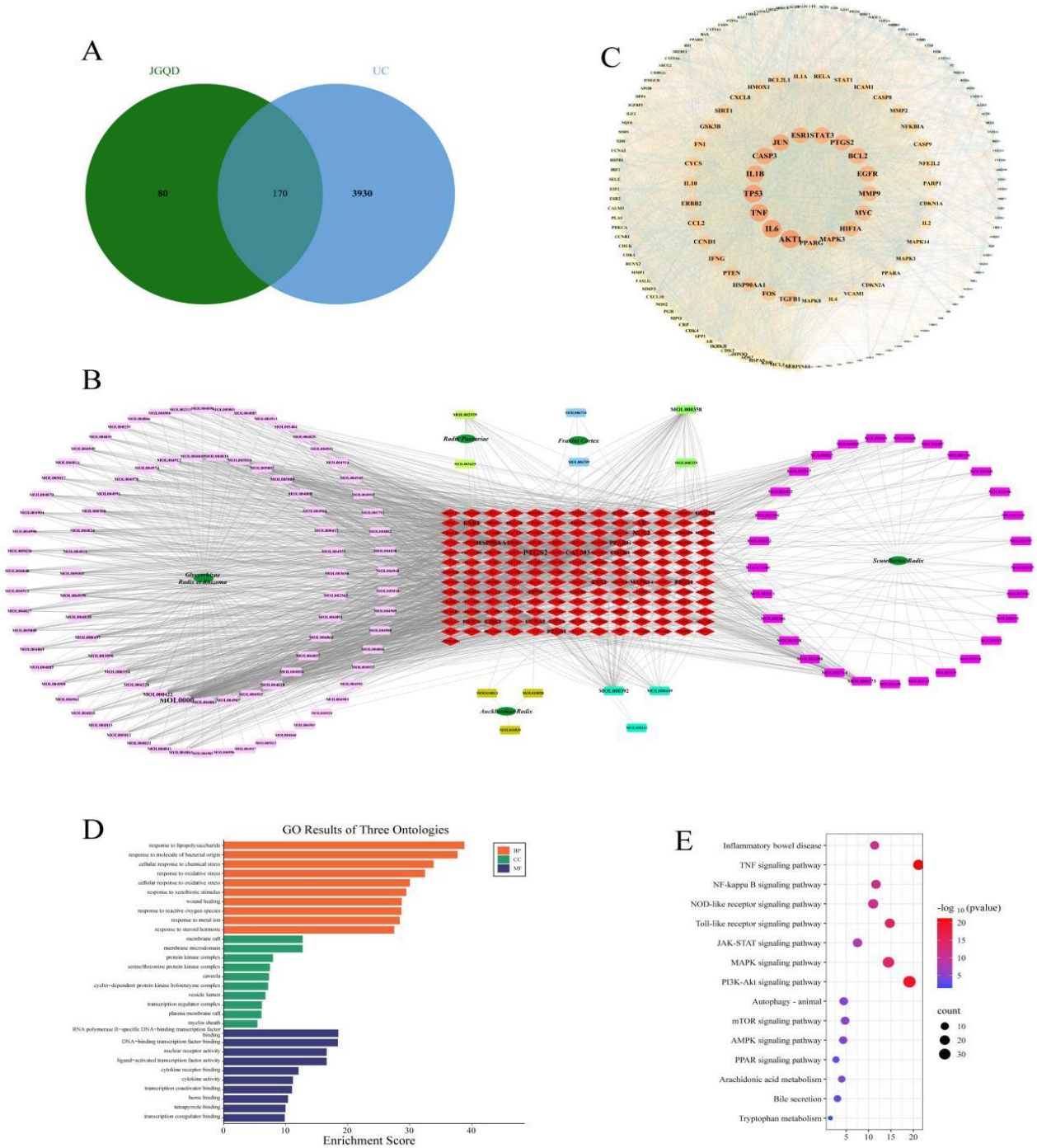

Fig. 1: Network pharmacology analysis of JGQD in the treatment of UC. (A) Venn diagram illustrating the overlap between JGQD-associated targets and UC-related therapeutic targets. (B) Drug–active component–disease target interaction network of JGQD against UC. Oval nodes represent individual herbal medicines within JGQD; rectangular nodes represent bioactive compounds, with different colors indicating their herbal origin; diamond-shaped nodes denote core target genes. (C) Protein–protein interaction (PPI) network of core therapeutic targets for UC. (D) Gene Ontology (GO) enrichment analysis of core therapeutic targets, including biological process (BP), cellular component (CC) and molecular function (MF) categories. (E) Kyoto Encyclopedia of Genes and Genomes (KEGG) pathway enrichment analysis of core therapeutic targets for UC.

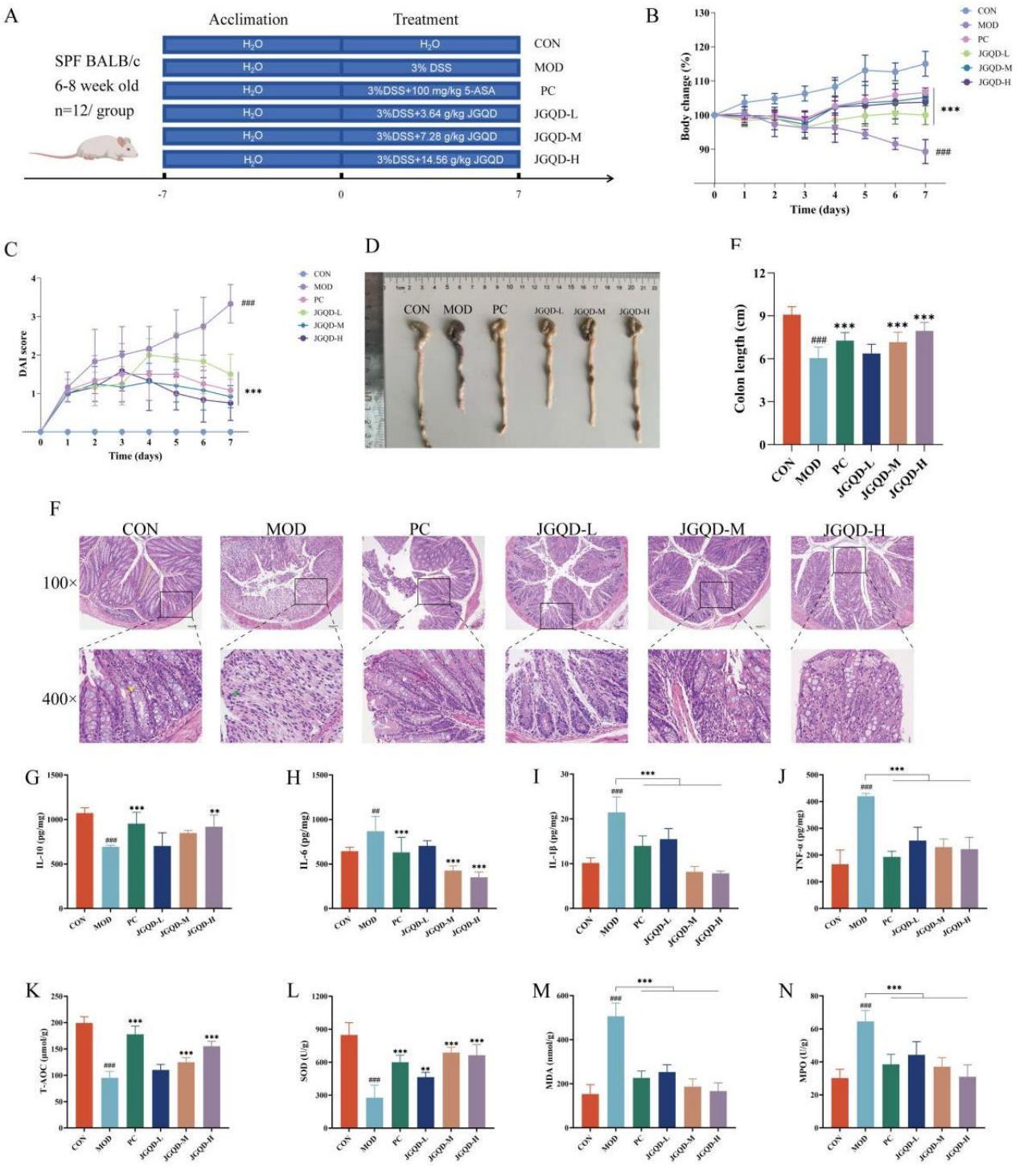

Fig. 2: JGQD alleviates colonic injury, inflammatory responses, and oxidative stress in DSS-induced UC mice. (A) Schematic diagram of the animal experimental design (n = 12 per group). (B) Changes in body weight among different groups. (C) Disease activity index (DAI) scores in different groups. (D–E) Colon length measurements in different groups. (F) Representative histopathological images of colonic tissues. Yellow dashed boxes indicate intact crypt architecture; yellow arrows indicate goblet cells; green arrows indicate lymphocyte infiltration (100×, scale bar = 100μm; 400×, scale bar=400μm). (G–J) Levels of inflammatory cytokines (IL-10, IL-6, IL-1β and TNF-α) in different groups. (K–N) Oxidative stress-related indicators (T-AOC, SOD, MDA and MPO) in different groups. Data are presented as mean ± SD. ##P<0.01 and ###P<0.001 versus the CON group; *P<0.05 and **P<0.01 versus the DSS group.

JGQD reduces inflammatory cytokine production and oxidative stress in the colon of UC mice: As illustrated in Fig. 2G–N, DSS administration triggered prominent elevations in colonic concentrations of IL-6, IL-1β, TNF-α, MDA and MPO relative to the control cohort, alongside drastic declines in IL-10, T-AOC and SOD activities (P<0.001). Such pathological alterations were effectively rescued following intervention with mesalazine (positive drug) and graded doses of JGQD. Relative to the untreated model group, animals receiving medium- and high-dose JGQD displayed remarkably suppressed pro-inflammatory cytokine and oxidative injury biomarker levels, accompanied by elevated anti-inflammatory IL-10 as well as enhanced antioxidant capacity (T-AOC and SOD) (P<0.01). Notably, the high-dose JGQD regimen exerted the most robust regulatory efficacy across all therapeutic subgroups.

JGQD Restores intestinal mucosal barrier integrity in UC mice: The safeguarding influence of JGQD on the integrity of the intestinal barrier was assessed by the measurement of TJ protein expression using immunofluorescence labelling and Western blotting. In contrast to the CON group, exposure to DSS markedly decreased the expression levels of Claudin-3, Occludin, and ZO-1 in colonic tissues (Fig. 3A–J; P<0.01), signifying a substantial compromise of epithelial barrier integrity.

JGQD modulates fecal microbiota composition and abundance in UC mice: The 16S rRNA gene was sequenced in faecal samples from the CON, MOD, and JGQD-H groups to investigate the gut microbiota composition. Alpha diversity metrics revealed comparable Sobs and Chao1 values across all three cohorts, yet significant intergroup disparities were detected in Shannon and Simpson estimators (P<0.05) (Fig. 4A–D), implying that DSS insult and subsequent JGQD intervention reshaped gut microbial diversity profiles. Non-metric multidimensional scaling (NMDS) plots displayed evident clustering separation between distinct experimental subgroups (stress value = 0.128) (Fig. 4E). ANOSIM and PERMANOVA statistical tests further corroborated this compositional divergence (P=0.001), confirming distinguishable microbial community architectures induced by DSS and JGQD treatment.

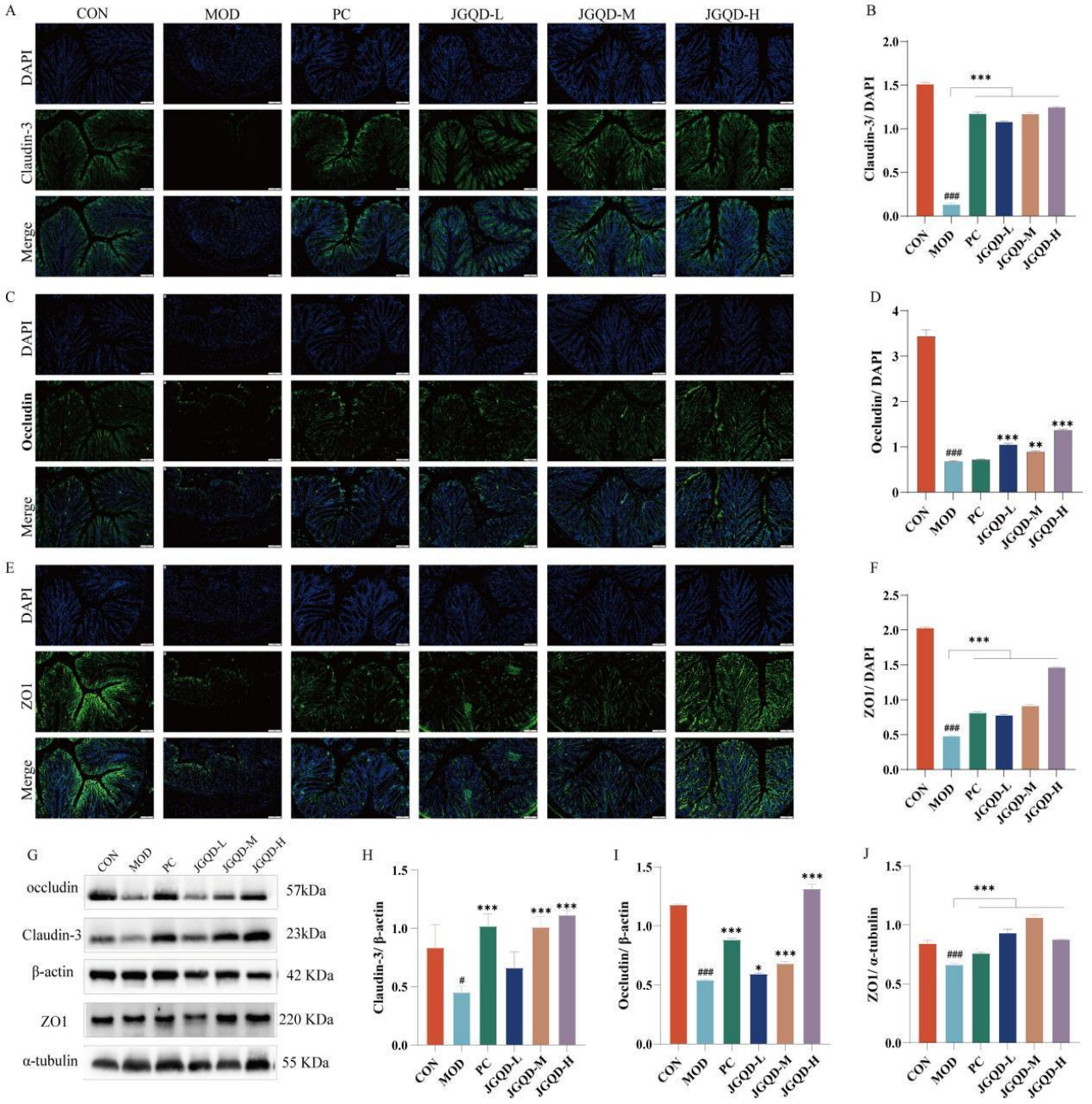

Fig. 3: JGQD attenuates colonic mucosal injury in DSS-induced UC mice. (A–F) Representative immunofluorescence images and quantitative analysis of tight junction proteins (Claudin-3, Occludin and ZO-1) in colonic tissues from different groups. Scale bar = 50μM. (G–J) Densitometric analysis of Claudin-3, ZO-1 and Occludin protein expression in colonic tissues from different groups, as determined by Western blotting. β-Actin and α-tubulin were used as internal loading controls. Data are presented as mean ± SD. #P<0.05, ##P<0.01 and ###P<0.001 versus the CON group; *P<0.05, **P<0.01 and ***P<0.001 versus the MOD group.

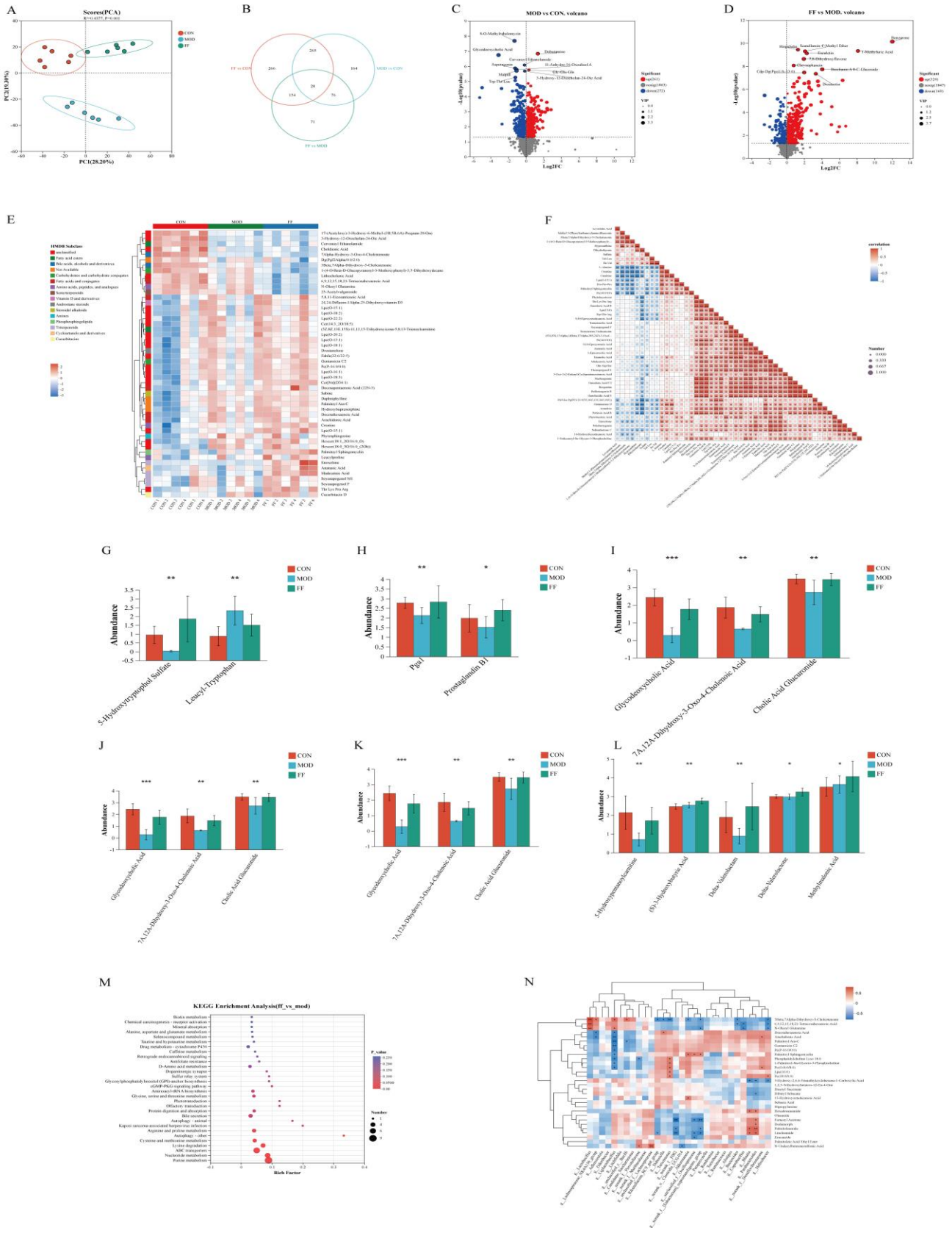

Fig. 4: JGQD modulates gut microbiota composition and abundance in DSS-induced UC mice. (A–D) Alpha diversity analysis of gut microbiota in different groups, including Sobs, Chao1, Shannon, and Simpson indices. (E) NMDS analysis of gut microbial communities among different groups. (F) Venn diagram showing shared and unique operational taxonomic units (ASVs) among different groups. (G) Relative abundance of gut microbiota at the phylum level. (H) Relative abundance of gut microbiota at the genus level. (I) LEfSe analysis of differential taxa among groups. (J) LDA scores derived from LEfSe analysis (LDA>2, P<0.05). (K) Differential microbial genera between the CON and JGQD-H groups analyzed by the Wilcoxon rank-sum test. (L) Differential microbial genera between the MOD and JGQD-H groups analyzed by the Wilcoxon rank-sum test. (M) Spearman rank correlation analysis among phenotypic indicators, colonic inflammatory cytokines, oxidative stress markers, and tight junction proteins across groups. (N) Spearman rank correlation analysis between the top 15 microbial genera in the JGQD-H group and phenotypic indicators, colonic inflammatory cytokines, oxidative stress markers, and tight junction proteins. Data are presented as mean ±SD. *P<0.05, **P<0.01 and ***P<0.001.

A total of 79 ASVs were shared by all three groups, whereas 18 ASVs were detected exclusively in the JGQD-H group (Fig. 4F). Bacillota was the most prevalent phylum in the CON group, as indicated by the phylum-level analysis (Fig. 4G). The abundance of Bacillota was reduced by DSS administration, while Bacteroidota, Thermodesulfobacteriota, and Campylobacterota were increased. Administration of JGQD-H alleviated DSS-induced microbial dysbiosis and enhanced the proliferation of Verrucomicrobiota. Genus-level analysis indicated that Lactobacillus was the most prevalent genus in the CON group (Fig. 4H). However, it was significantly diminished in the MOD group, which was characterized by an increase in norank_f__Muribaculaceae, Bacteroides, and norank_f__Desulfovibrionaceae. Additional alterations were observed in Dubosiella and Paraprevotella, while the abundance of Lactobacillus was increased and norank_f__Muribaculaceae was reduced because of JGQD-H treatment. Characteristic microbial biomarkers were additionally identified among the three groups through LEfSe analysis (Fig. 4I, J). The CON group was enriched in Bacillota, specifically Lactobacillales, Lactobacillaceae, and Lactobacillus, while the MOD group exhibited enrichment of taxa from the Bacteroidota, Desulfovibrionaceae, and Thermodesulfobacteriota. LEfSe analysis indicated that Verrucomicrobiota and Pseudomonadota were characteristic taxa of the JGQD-H group, whereas Akkermansia was identified as the major discriminative genus. Wilcoxon rank-sum analysis further confirmed significant differences in microbial composition (Fig. 4K, L). In contrast to the MOD group, JGQD-H treatment markedly elevated the relative abundances of Akkermansia, norank_f__F082, Turicimonas, Acutalibacter and Escherichia-Shigella ($P<0.05$). Among these taxa, Akkermansia showed the greatest enrichment following JGQD treatment and exceeded the levels observed in both the CON and MOD groups.

JGQD enriches akkermansia and is associated with improved intestinal outcomes in UC mice: To identify pairwise correlations between molecular and phenotypic indicators associated with UC, a Spearman's rank correlation test was employed (Fig. 4M). Significant positive interrelationships were observed between colon length, body weight, anti-inflammatory IL-10, antioxidant biomarkers (T-AOC and SOD), and the protein abundances of tight junction components Claudin-3, Occludin, and ZO-1 ($P<0.05$). This suggested a coordinated restoration of epithelial barrier function, antioxidant defence capacity, and anti-inflammatory status.

Spearman correlation analysis was employed to establish a connection between the top 15 prevalent genera in the high-dose JGQD cohort and intestinal health biomarkers to further investigate the role of gut microorganisms in mucosal recovery (Fig. 4N). Only Akkermansia exhibited significant positive correlations with tight junction protein expression, body weight, colon length, and antioxidant activity (T-AOC, SOD) among all tested taxa ($P<0.05$). Concurrently, this genus exhibited significant negative correlations with DAI scores, pro-inflammatory mediators and oxidative damage markers ($P<0.05$). In contrast, Romboutsia exhibited an inverse correlation profile, indicating negative connections with all markers that represent intestinal homeostasis.

Microbial composition analysis further confirmed these results. In contrast to the MOD group, JGQD-H therapy markedly elevated the relative abundance of Akkermansia while diminishing that of Romboutsia. In mice treated with DSS, the enrichment of Akkermansia was linked to improvements in disease severity and colitis-related pathological indicators.

JGQD reshapes the fecal metabolomic landscape in UC mice: Untargeted fecal metabolomics was performed to characterize metabolic changes induced by JGQD intervention (Fig. 5). PCA revealed distinct metabolic clustering and low intra-group variability among the CON, MOD and JGQD-H groups (Fig. 5A). A total of 2336 metabolites were identified. The MOD group exhibited 533 differential metabolites (261 upregulated, 272 downregulated) relative to CON, while JGQD-H treatment altered 489 metabolites (320 upregulated, 169 downregulated) (Fig. 5B–5C). DSS exposure primarily disrupted bile acid, lipid, amino acid, and peptide metabolism, with significant depletion of glycodeoxycholic acid and 3-hydroxy-12-oxocholan-24-oic acid. In contrast, JGQD-H supplementation enriched flavonoid metabolites including hispidulin, esculetin, and diosmetin and partially restored DSS-triggered lipid metabolic disorders.

HMDB subclass annotation classified the differential metabolites into amino acid-related metabolites, oxidative stress-associated metabolites, tryptophan derivatives, arachidonic acid-derived lipid mediators, bile acid-related metabolites, and short-chain fatty acids (Fig. 5D). JGQD-H treatment partially restored these metabolic alterations, whereas the MOD group exhibited marked disturbances in lipid metabolism, amino acid metabolism, and redox-related metabolites in comparison to the CON group. Pearson correlation analysis revealed distinct metabolic clusters, with strong positive correlations among metabolites within the same functional categories and negative correlations between different metabolite classes (Fig. 5E). Lipid mediators, particularly arachidonic acid derivatives and other polyunsaturated fatty acids, formed highly correlated clusters and were negatively associated with amino acid- and short-chain fatty acid-related metabolites. Targeted metabolite analysis further confirmed significant alterations in tryptophan metabolism, bile acid metabolism, oxidative stress-related metabolites, lipid mediators, and amino acid metabolism (Fig. 5F–K). The levels of 5-hydroxykynurenine, 5-hydroxytryptophol sulphate, glycodeoxycholic acid, cholic acid glucuronide, lysine- and taurine-related metabolites, and uric acid were significantly restored by JGQD-H in comparison to the MOD group, while hypoxanthine and dihydrolipoate were reduced ($P<0.05$).

Functional annotation derived from KEGG analysis indicated that metabolites sensitive to JGQD were mostly engaged in amino acid metabolism, nucleotide metabolism, bile secretion, protein digestion and absorption, ABC transporters, and autophagy-related pathways (Fig. 5L). Additional correlation analysis verified the close relationship between differential metabolites and intestinal microbiota (Fig. 5M). Akkermansia was positively correlated with 8,11-eicosatrienoic acid and L-alanine, whereas Escherichia-Shigella exhibited positive associations with arachidonic acid ($P<0.05$).

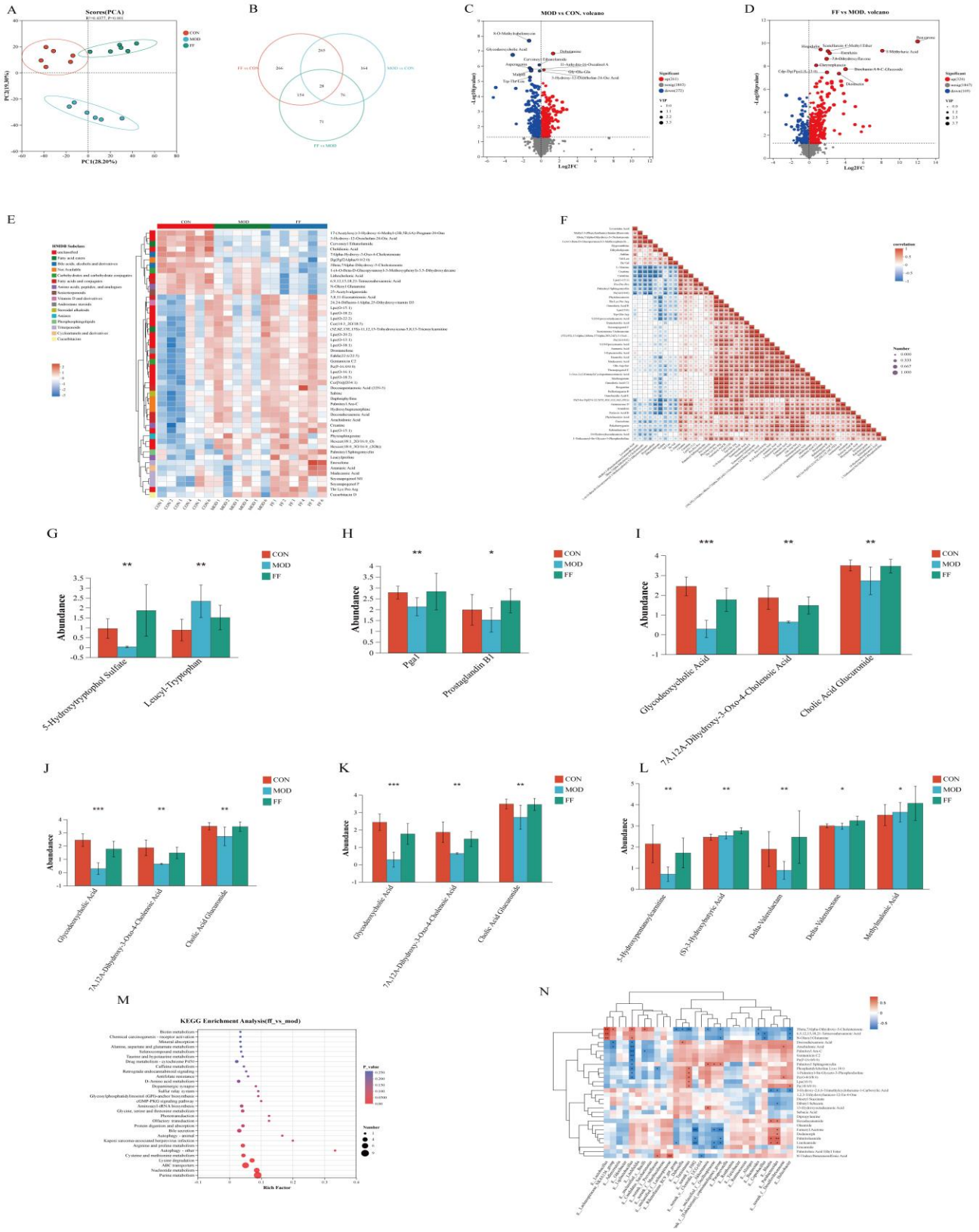

Fig. 5: JGQD alters the composition and abundance of fecal metabolites in DSS-induced UC mice. (A) Principal component analysis (PCA) of fecal metabolomic profiles among different groups. (B) Differential metabolites identified in the MOD group compared with the CON group. (C) Differential metabolites identified in the JGQD-H group compared with the MOD group. (D) Heatmap showing the relative abundance of the top 50 metabolites in fecal samples across groups. (E) Spearman rank correlation analysis among the top 50 metabolites in fecal samples from different groups. (F) Kruskal–Wallis rank-sum test analysis of differential short-chain fatty acid metabolites among groups. (G) Kruskal–Wallis rank-sum test analysis of differential arachidonic acid–related metabolites among groups. (H) Kruskal–Wallis rank-sum test analysis of differential bile acid–related metabolites among groups. (I) Kruskal–Wallis rank-sum test analysis of differential oxidative stress–related metabolites among groups. (J) Kruskal–Wallis rank-sum test analysis of differential amino acid–related metabolites among groups. (K) Kruskal–Wallis rank-sum test analysis of differential tryptophan metabolism–related metabolites among groups. (L) KEGG pathway enrichment analysis of differential metabolites in the JGQD-H group compared with the MOD group. (M) Pearson correlation analysis between dominant metabolites and dominant microbial genera in the JGQD-H group. Data are presented as mean ±SD. *P<0.05, **P<0.01 and ***P<0.001.

DISCUSSION

The classical Gegen Qinlian Decoction is traditionally prescribed for clearing heat, eliminating toxins, drying dampness and relieving dysentery, and has demonstrated clinical efficacy in alleviating diarrhea and mucosal inflammation during the acute phase of UC characterized by damp–heat accumulation (Lu*et al*. 2021, Wang*et al*. 2023). Recent advancements in the comprehension of ulcerative colitis pathogenesis have established the condition as a multifactorial disorder characterized by persistent mucosal inflammation, abdominal pain, intestinal dysmotility, epithelial barrier disruption, and gut microbiota dysbiosis (Hirten and Sands, 2021, Le Berre and Peyrin-Biroulet, 2021). The JGQD used in the present study incorporates Aucklandiae Radix and Fraxini Cortex, with Glycyrrhizae Radix et Rhizoma as a harmonizing component, thereby expanding the functional scope of the original formula to address these interconnected pathological processes. From the perspective of classical prescription theory, this formulation integrates therapeutic principles derived from Xianglian Pill (emphasizing heat-clearing and qi-regulating analgesia) and Baitouweng Decoction (focusing on detoxification and intestinal mucosal protection). The retention of the anti-inflammatory and antidiarrheal properties of Radix Puerariae and Scutellariae Radix, coupled with the inclusion of Aucklandiae Radix, may facilitate the alleviation of abdominal pain and enhancement of intestinal motility, while Fraxini Cortex may augment anti-inflammatory, antibacterial, and mucosal-protective effects (Pan, Wang *et al*., 2024; Yang, Deng *et al*., 2024). Glycyrrhizae Radix et Rhizoma likely supports immune modulation and tissue repair, collectively enabling broader coverage of key pathological features of modern UC (Shi *et al*., 2022).

By identifying numerous inflammation-related signalling pathways, such as TNF, NF-κB, PI3K-Akt, MAPK, JAK-STAT, Toll-like receptor and NOD-like receptor pathways, network pharmacology analysis substantiated the pharmacological basis of JGQD. These findings align with the traditional multi-faceted and multi-target attributes of JGQD. The impact of JGQD on inflammatory reactions and oxidative stress was also assessed in mice suffering from DSS-induced colitis. In contrast to the MOD group, JGQD therapy markedly decreased colonic concentrations of TNF-α, IL-6, IL-1β, MDA and MPO, while elevating levels of IL-10, SOD and T-AOC. These results suggest that JGQD mitigates intestinal inflammation and oxidative stress generated by DSS (Peng Y *et al*., 2024). Parallel to this, JGQD reduced MDA and MPO levels and elevated SOD activity and T-AOC, indicating that oxidative stress was mitigated and antioxidant capacity was improved. Reduced MPO reflects decreased neutrophil infiltration, whereas restoration of SOD activity indicates improved antioxidant defense against DSS-induced oxidative injury (Choudhary *et al*., 2001; Stupin *et al*., 2017; Zheng *et al*., 2017).

Inflammation and oxidative stress significantly contribute to the compromise of the intestinal epithelial barrier in colitis. JGQD reinstated the expression of ZO-1, Occludin and Claudin-3, signifying enhanced tight junction integrity. Prior research has demonstrated that inflammatory mediators and oxidative stress can stimulate NF-κB and MAPK signaling pathways, thus impairing tight junction architecture and elevating epithelial permeability (Li *et al*., 2014; Dai *et al*., 2025). Consequently, the JGQD-induced attenuation of inflammation and oxidative dysregulation may facilitate the restoration of intestinal barrier equilibrium.

Improved barrier integrity was accompanied by alterations in gut microbiota composition (Chopyk and Grakoui, 2020), consistent with previous studies showing that fucoidan and artemisinic acid alleviated experimental intestinal inflammation alongside improvements in inflammatory, oxidative, histopathological, and microbial profiles (Peng S *et al*., 2024; Wang *et al*., 2026). The JGQD therapy significantly altered the composition of the microbial community, as demonstrated by an increase in Akkermansia and a decrease in Romboutsia, a species that is linked to dysbiosis and inflammatory conditions. Correlation study revealed substantial relationships between Akkermansia prevalence and inflammatory cytokines, oxidative stress indicators and tight junction protein levels. Akkermansia is recognized for its ability to inhabit the mucus layer, facilitate mucin turnover, strengthen epithelial barrier integrity and influence host immunological responses, notably through the elevation of ZO-1 and Claudin expression (Liu *et al*., 2022). The present findings further support its potential contribution to JGQD-mediated intestinal recovery. Metabolomics analysis revealed systemic metabolic reprogramming induced by JGQD. Differential metabolites exhibited modular organization, with coordinated alterations across lipid, amino acid, bile acid and tryptophan-related pathways. Arachidonic acid-derived lipid mediators formed tightly connected metabolic clusters and displayed inverse relationships with amino acid and short-chain fatty acid-associated metabolites, suggesting antagonistic regulation between proinflammatory lipid pathways and energy/anti-inflammatory metabolic circuits. Targeted quantification confirmed that JGQD reversed DSS-induced abnormalities in tryptophan derivatives, bile acid metabolites, oxidative stress-related lipids, and amino acid metabolites. These metabolic changes were highly consistent with inflammation- and metabolism-related pathways identified by network pharmacology analysis. The KEGG enrichment analysis also demonstrated that differential metabolites were primarily associated with transport-related pathways, bile secretion, nucleotide metabolism and amino acid metabolism. This suggests that JGQD modulated multiple metabolic processes involved in intestinal homeostasis (Wang *et al*., 2023). Microbiota–metabolite correlation analysis demonstrated coordinated associations between beneficial taxa such as Akkermansia and anti-inflammatory lipids and energy-related amino acids, whereas potentially pathogenic genera correlated positively with proinflammatory lipid precursors. These findings indicate that JGQD may effectively address UC by meticulously modulating the microbiota–metabolite axis. This procedure leads to diminished inflammation and oxidative stress, reinstatement of tight junction protein expression, improvement of mucosal permeability and interruption of the harmful cycle of inflammatory escalation.

Collectively, our findings indicate that JGQD stimulates DSS-induced colitis by orchestrating the regulation of inflammation, oxidative stress, intestinal barrier function, gut microbiota and host metabolism. The intricate regulatory framework that supports the therapeutic benefits of JGQD in ulcerative colitis is validated by the integration of experimental findings with network pharmacology predictions.

Author contribution statement: QY, YH: Investigation, Data curation, Formal analysis, Writing – original draft, Visualization; YG, XC: Methodology, Validation, Investigation; XY: Resources, Software, Data curation; XY: Reviewing & editing; XW, NL, QZ: Conceptualization, Funding acquisition, Project administration, Supervision, Writing – review & editing.

Fundings: This research was financially supported by the National Natural Science Foundation of China (Grant No. 32604666) (Qiu Zhong), the Natural Science Foundation of Guangxi (Grant No. 2023GXNSFBA026354), and the Yunnan Key Laboratory of Veterinary Etiological Biology (Grant No. 202449CE340019) (Junjun He)

Acknowledgements: We appreciate the assistance from our distinguished colleagues in Guangxi Key Laboratory of Animal Breeding, Disease Control and Prevention of Guangxi University and Department of Clinic Veterinary of Yunnan Agricultural University.

Declaration of competing interest: None.

REFERENCES

Abraham C, Abreu MT, Turner JR, 2022. Pattern recognition receptor signaling and cytokine networks in microbial defenses and regulation of intestinal barriers: Implications for inflammatory bowel disease. Gastroenterology 162:1602-1616.e1606.

Bi WY, Sun JT, Zhang Y, *et al*., 2025. Protective role of lotus leaf polysaccharides in mice with ulcerative colitis. Pakistan Veterinary Journal 45:1662-1673.

Chopyk DM, Grakoui A, 2020. Contribution of the intestinal microbiome and gut barrier to hepatic disorders. Gastroenterology 159:849-863.

Choudhary S, Keshavarzian A, Yong S, *et al*., 2001. Novel antioxidants zolimid and AEOL11201 ameliorate colitis in rats. Digestive Diseases and Sciences 46:2222-2230.

Dai S, Li C, Li D, *et al*., 2025. α-Glycerol monolaurate promotes tight junction proteins expression through PKC/MAPK/ATF-2 signaling pathway. Frontiers in Nutrition 12:1598991.

Hirten RP, Sands BE, 2021. New Therapeutics for ulcerative colitis. Annual Review of Medicine 72:199-213.

Hu Y, Tang J, Xie Y, *et al*., 2024. Gegen Qinlian decoction ameliorates TNBS-induced ulcerative colitis by regulating Th2/Th1 and Tregs/Th17 cells balance, inhibiting NLRP3 inflammasome activation and reshaping gut microbiota. Journal of Ethnopharmacology 328:117956.

Huang Y, Liu Q, Lu SR, *et al*., 2026. Modulatory effects of cordyceps militaris polysaccharides on metabolic dysregulation and gut microbiota in high-fat diet-induced obesity in mice. ES Food and Agroforestry 23:2059.

Jergens AE, Heilmann RM, 2022. Canine chronic enteropathy—Current state-of-the-art and emerging concepts. Frontiers in Veterinary Science 9:923013.

Kaga C, Kakiyama S, Hokkyo A, *et al*., 2024. Characterization of faecal microbiota, organic acids and serum inflammatory markers in dogs with chronic enteropathy and intestinal lymphoma. Scientific Reports 14:19387.

Le Berre C, Peyrin-Biroulet L, 2021. Selecting end points for disease-modification trials in inflammatory bowel disease: the SPIRIT Consensus from the IOIBD. Gastroenterology 160:1452-1460.e1421.

Li J, Zhong W, Wang W, *et al*., 2014. Ginsenoside metabolite compound K promotes recovery of dextran sulfate sodium-induced colitis and inhibits inflammatory responses by suppressing NF-κB activation. PLOS ONE 9:e87810.

Liu C, Zhao D, Ma W, *et al*., 2016. Denitrifying sulfide removal process on high-salinity wastewaters in the presence of Halomonas sp. Applied Microbiology and Biotechnology 100:1421-1426.

Liu MJ, Yang JY, Yan ZH, *et al*., 2022. Recent findings in Akkermansia muciniphila-regulated metabolism and its role in intestinal diseases. Clinical Nutrition 41:2333-2344.

Liu Y, Li BG, Su YH, *et al*., 2022. Potential activity of traditional Chinese medicine against ulcerative colitis: A review. Journal of Ethnopharmacology 289:115084.

Loh JS, Mak WQ, Tan LKS, *et al*., 2024. Microbiota-gut-brain axis and its therapeutic applications in neurodegenerative diseases. Signal Transduction and Targeted Therapy 9:37.

Lu JZ, Ye D, Ma BL, 2021. Constituents, pharmacokinetics, and pharmacology of Gegen-Qinlian decoction. Frontiers in Pharmacology 12:668418.

Meng A, Zhang X, Pubu P, *et al.,* 2024. Protective effect of lentinan against LPS-induced injury in mice via influencing antioxidant enzyme activity, inflammatory pathways, and gut microbiota. Pakistan Veterinary Journal 44(3):647–656.

Pan SM, Wang CL, Hu ZF, *et al*., 2024. Baitouweng decoction repairs the intestinal barrier in DSS-induced colitis mice via regulation of AMPK/mTOR-mediated autophagy. Journal of Ethnopharmacology 318:116888.

Parada Venegas D, De la Fuente MK, Landskron G, *et al*., 2019. Short chain fatty acids (SCFAs)-mediated gut epithelial and immune regulation and its relevance for inflammatory bowel diseases. Frontiers in Immunology 10:277.

Peng S, Xu C, He Q, *et al*., 2024. Fucoidan alleviates intestine damage in mice induced by LPS via regulation of microbiota. Pakistan Veterinary Journal 44(2):517–525.

Peng Y, Zhu J, Li Y, *et al*., 2024. Almond polysaccharides inhibit DSS-induced inflammatory response in ulcerative colitis mice through NF-κB pathways. International Journal of Biological Macromolecules 281:136206.

Perler BK, Ungaro R, Baird G, *et al*., 2019. Presenting symptoms in inflammatory bowel disease: descriptive analysis of a community-based inception cohort. BMC Gastroenterology 19:47.

Prasad S, Mingrino R, Kaukinen K, *et al*., 2005. Inflammatory processes have differential effects on claudins 2, 3 and 4 in colonic epithelial cells. Laboratory Investigation 85:1139-1162.

Shahgoli VK, Noorolyai S, Ahmadpour Youshanlui M, *et al*., 2024. Inflammatory bowel disease, colitis, and cancer: unmasking the chronic inflammation link. International Journal of Colorectal Disease 39:173.

Sharma B, Agriantonis G, Twelker K, *et al*., 2025. Gut microbiota serves as a crucial independent biomarker in inflammatory bowel disease (IBD). International Journal of Molecular Sciences 26:2503.

Shi G, Kong J, Wang Y, *et al*., 2022. Glycyrrhiza uralensis Fisch. alleviates dextran sulfate sodium-induced colitis in mice through inhibiting of NF-κB signaling pathways and modulating intestinal microbiota. Journal of Ethnopharmacology 298:115640.

Stupin A, Cosic A, Novak S, *et al*., 2017. Reduced dietary Selenium impairs vascular function by increasing oxidative stress in sprague-dawley rat aortas. International Journal of Environmental Research and Public Health 14:591.

Ungaro R, Mehandru S, Allen PB, *et al*., 2017. Ulcerative colitis. The Lancet 389:1756-1770.

Wang J, Zhu N, Su X, *et al*., 2023. Gut-microbiota-derived metabolites maintain gut and systemic immune homeostasis. Cells 12:793.

Wang L, Zheng XH, Shoaib M, *et al*., 2026. Multidimensional evaluation of artemisinic acid against colitis in murine model: Integrating microbiota remodeling, histopathological improvement and inflammation regulation. Pakistan Veterinary Journal 46:169-178.

Wang M, Fu R, Xu D, *et al*., 2024. Traditional Chinese medicine: A promising strategy to regulate the imbalance of bacterial flora, impaired intestinal barrier and immune function attributed to ulcerative colitis through intestinal microecology. Journal of Ethnopharmacology 318:116879.

Wang X, Quan J, Xiu C, *et al*., 2023. Gegen Qinlian decoction (GQD) inhibits ulcerative colitis by modulating ferroptosis-dependent pathway in mice and organoids. Chinese Medicine 18:110.

Wu B, Su S, Li Y, *et al*., 2025. Dysregulated programmed cell death of intestinal epithelial cells in ulcerative colitis: Molecular mechanisms and novel therapeutic interventions (Review). International Journal of Molecular Medicine 56:230.

Xu H, Zhu J, Lin X, *et al*., 2025. A Comprehensive review of traditional Chinese medicine in the management of ulcerative colitis. The American Journal of Chinese Medicine 53:435-473.

Yang L, Deng F, Gong Q, *et al*., 2024. Distribution of the active components from Xianglian Pill in tissues of healthy and antibiotic-associated diarrhea model mice and the mechanism study. Journal of Pharmaceutical and Biomedical Analysis 248:116326.

Yao D, Dai W, Dong M, *et al*., 2021. MUC2 and related bacterial factors: Therapeutic targets for ulcerative colitis. EBioMedicine 74:103751.

Zhao Y, Luan H, Jiang H, *et al*., 2021. Gegen Qinlian decoction relieved DSS-induced ulcerative colitis in mice by modulating Th17/Treg cell homeostasis via suppressing IL-6/JAK2/STAT3 signaling. Phytomedicine 84:153519.

Zheng XY, Lv YF, Li S, *et al*., 2017. Recombinant adeno-associated virus carrying thymosin β(4) suppresses experimental colitis in mice. World Journal of Gastroenterology 23:242-255.

Zong Y, Meng J, Mao T, *et al*., 2023. Repairing the intestinal mucosal barrier of traditional Chinese medicine for ulcerative colitis: a review. Frontiers in Pharmacology 14:1273407.